Arab J Geosci (2016) 9: 373
DOI 10.1007/s12517-015-2188-6

ORIGINAL PAPER

GIS-based weights of evidence modeling applied to mineral prospectivity mapping of Sn-W and rare metals in Laouni area, Central Hoggar, Algeria

Hocine Zeghouane[1,3] · **Karim Allek**[2] · **Mokrane Kesraoui**[3]

Received: 23 May 2015 / Accepted: 15 October 2015 / Published online: 26 April 2016

Abstract The development in the emerging technologies of information and communications requires more rare metals. The existing resources, insufficient to assume this progress, require further investigations to discover new rare metal deposits. The traditional methods, based on manual overlay, are unsuitable and expensive. Thus, mineral exploration requires updated methods to easily, quickly, and cost effectively delineate new promising exploration zones. Geographical Information System (GIS) and applied geomatics provide and perfect various modeling techniques implemented in GIS software. In recent years, two spatial modeling techniques were developed and widely applied in mineral exploration, data-driven methods, and knowledge methods. Weight of evidence (WofE) is a data-driven method based on the Bayesian theorem and its fundamental concept of prior and posterior probabilities. The method combines statistically diverse geodata that represent ore-controlling factors by weighting their evidence using "control points" to create a "posterior probability map." Our study area, located at the southern part of Hoggar in the south of Algeria, is potential for Sn, W, and rare metals and encloses several deposits related to peraluminous post-orogenic rare metal granitoïds (RMGs). In this work, "weights of evidence" modeling is applied to map mineral potential of this style of mineralization. Seventeen predictor maps, representing the deposit recognition criterion model, were generated from multi-source geodata (lithology, geochemistry, tectonic, magmatism, and geophysics). These data were used as "input data" and the known deposits (48 mineral occurrences) as "training sites." The WofE modeling gets the following results: (1) generate an output map called "mineral potential map" (MPM), where potential zones are reduced to small areas; (2) the MPM efficiently predicts the well-known deposits of Nahda, Sedis, Rechla, and Tit N'Enir; and (3) highlights some unrecognized areas such as Tedjrine, Monts de Tessalit, and Gara Akeboum. (4) The control model demonstrates the possibility to extend the WofE method to the adjacent regions enclosing a small number of known mineral deposits.

Keywords Geomatic modeling · GIS · Prospectivity modeling · Weights of evidence · Mineral exploration · Rare metals · Hoggar

✉ Hocine Zeghouane
hocinezeghouane@yahoo.fr

[1] Department of Earth and Universe Sciences, University of Tizi Ouzou Algreia, Tizi Ouzou, Algeria

[2] Laboratory of Physics of the Earth, University of Boumerdès, Boumerdès, Algeria

[3] Laboratory of Metallogeny and Magmatism of Algeria, USTHB University, Isser, Algeria

Introduction

Because of the limits of the conventional methods based on traditional manual overlay processes, mineral exploration require nowadays the use of updated and innovative geomatic approaches. In fact, these methods are focused on the integration and combination in a Geographical Information System (GIS) environment of various geodatasets to identify efficiently new mineral targeting zones. Recent years have witnessed a great deal of interest for the application of GIS-based predictive spatial analysis techniques in order to integrate several exploration datasets in the framework of different deposit models for mineral potential mapping.

Based on a manner of weighting evidence, Bonham-Carter (1994) described predictive analysis techniques as knowledge-driven and data-driven models. Knowledge-driven models are more suitable for underexplored or unexplored areas characterized by few number of deposits (Porwal et al. 2006a; Bonham-Carter 1994; Carranza 2009). They use mathematical theories (e.g., Boolean operators, fuzzy logic, and Dumpster-Shafer belief functions), centered on the knowledge of the geologist explorer, where weighting evidence depends on experts' opinions. However, in data-driven models, the weights are calculated using statistical methods that quantify the spatial relationships between the evidential layers and the training sites (control points). These models, more appropriate for moderate to well-studied areas with a reasonably large number of known deposits (Porwal et al. 2006b; Carranza 2009), are based on several techniques such as logistic regression, artificial neural network, and weights of evidence (Harris et al. 2001).

The weights of evidence model is a Bayesian statistical method that uses the conditional probabilities to predict a hypothesis about the occurrence of an event based on the combination of known information in a study area where sufficient data are available to estimate the relative importance of each the information. In the recent years, it has been applied in several domains such as archeology (Diggs and Brunswig 2010), landslide susceptibility analysis and hazard (Mathew et al. 2007; Barbieri and Cambuli 2009; Hyun-Joo and Saro 2010), biology (Wildman and Peters 2008), geothermal potential (Yousefi and Kamkar-Rouhani 2004), and forests and fires (Romero-Calcerrada et al. 2008; Fagin and Hoagland Bruce 2010). It has also been used to map mineral potential of a variety of mineral resources such as Cu-Pb-Zn (Benomar and Fuling 2006), VMS Cu-Au (Partington 2010), gold potential (Carranza 2009; Ziaii et al. 2009; Nykänen and Salmirinne 2007; Nykänen et al. 2011), and magmatic nickel sulfide (Porwal 2010). In this work, it will be used to map mineral potential of tin-wolfram (Sn-W) and rare metal mineralization in the Laouni area (Hoggar shield, Algeria).

The Laouni region, also known as "*Laouni rare metal province*," is characterized by the abundance of rare metal mineralization associated with peraluminous rare metal granitoïds (RMGs). Over the past decades, discoveries and prospecting breakthroughs have received a significant attention. The study area encloses several known mineral occurrences represented by deposits and prospects. However, previous works are focused mainly on conducting intensive geochemical testing of the surface by collecting a grid of samples over the areas which are amenable to soil geochemistry testing. In addition, conventional methods are based on personal experience and interpretation of existing geological, geochemical, or geophysical data (e.g., Lelubre 1952; Boissonnas 1973; Benazouz-Fezoui 1989; Chalal 1989; Azzouni-Sekkal 1990; Djadoun 1993; Chillak et al. 1986; Al 1990; Kesraoui 2006).

The main purpose of this study is the application of the weights of evidence modeling by combining multi-source geospatial data in a GIS environment for the assessment of Sn-W and rare metal potential. The aim is to increase the chances of finding deposit sites within the Laouni region. This outcome has a great number of advantages, including maximizing processing efficiency, easy interpretability, and improved decision making.

The method encloses also some disadvantages such as the use of binary maps which may result in loss or distortion of valuable information. This is corrected by the introduction of the "extended weight of evidence (WofE)" (Porwal et al. 2001) and fuzzy WofE (Porwal et al. 2006) and modified fuzzy WofE (Zhang et al. 2014). In recent years, the uncertainty of mineral potential map (MPM) due to missing evidence was advantageously studied (Zuo et al. 2015).

This article goes through the following three crucial aspects: first, various types of geodatasets are selected carefully and are processed for building the WofE model. Second, quantitative analysis of spatial association between evidential layers and the known Sn-W-rare metal (RM) mineralization is exposed for better understanding of the ore-controlling factors. Last but not least, the resultant mineral prospectivity map is validated using "test deposits."

Geological background of the study area

The Laouni study region is located at the southern part of Hoggar, in south Algeria. It is bounded by latitudes 20–21°N and longitudes 5–6°E. Geologically speaking, it belongs to the central part of Hoggar which constitutes the Air and the Adrar of Iforas of the Tuareg shield interpreted as the result of a complete Wilson cycle which occurred between 800 and 600 Ma (Black et al. 1979; Caby et al. 1981). Previous studies (Black et al. 1994; Liegeois et al. 2003) show that the Hoggar shield is made of 23 terranes limited by mega-shear zones and basal thrusts. Four of them, namely, Laouni, Azrou-N'Fad, Tefedest, and Egéré-Aleksod, grouped under the acronym "LATEA" (Liegeois et al. 2003), are made principally of Proterozoic basement with basic features (Bertrand et al. 1986). Our study region is part of this large structural unit (Fig. 1).

The simplified geological map of the Laouni area (Fig. 2) shows eight main geological units. Units (i) and (ii) correspond to Paleoproterozoic metamorphic series made mainly of gneiss and metasediments metamorphosed under amphibolite or granulite facies. Unit (iii) consists of Neoproterozoic rocks enclosing volcano-clastic series bounded generally by tectonic contacts (Bertrand and Caby 1978). Units (iv) and (v) are essentially composed by Pan-African migmatites and syn-kinematic granitic batholiths (>70 % surface), intruded in metamorphic country rocks with sub-horizontal foliation dated between 600 and 630 Ma (Bertrand et al. 1986). Unit (vi) consists of mafic-ultramafic rocks, interpreted as ophiolitic remnants (Black et al. 1994) intrusive into syn-kinematic granites and Neoproterozoic metamorphic rocks and emplaced between 600 and 520 Ma (Cottin et

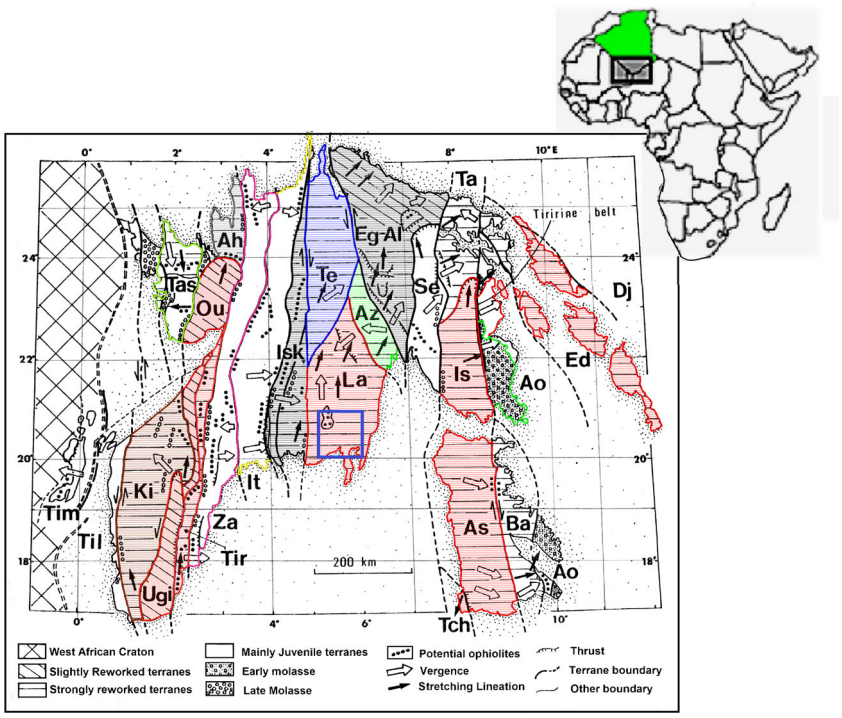

Fig. 1 Tuareg shield terrane map (Black et al. 1994): Djanet (Dj), Edembo (Ed), Aouzegueur (Ao), Barghot (Ba), Assode-Issalane (As-Is), Tchilit (Tch), Tazat (Ta), Serouenout (Se), Egere-Aleksod (Eg-Al), Azrou-n-Fad (Az), Tefedest (Te), Laouni (La), Iskel (Isk), In Teidini (It), Tin Zaouatene (Za), Tirek (Tir), Ahnet (Ah), In Ouzzal (Ou), Iforas granulitic unit (Ugi), Tassendjanet (Tas), Kidal (Ki), Tilemsi (Til), and Timetrine (Tim)

al. 1998). Unit (vii) is post-orogenic albite-topaz bearing granitic intrusions related to the "Taourirt magmatism" dated at 525 Ma and all linked to late movements along mega-shear zones (Black et al. 1994) that are relatively abundant in the Tuareg shield and to which Sn-W and rare metal mineralization are strongly associated. Unit (viii) is represented by Paleozoic sedimentary covers of platform type.

Weights of evidence theory

The WofE is a Bayesian statistical method that uses conditional probabilities to determine the relative importance of occurrence "evidence." An exhaustive explanation of the mathematical formulation of the WofE modeling method is revealed in Bonham-Carter (1989, 1994), Wang and Al (2002), and Carranza (2009).

WofE calculations are based on prior and posterior concept of probabilities. Prior probability, noted $P(D)$, is defined as the probability of a given number of unit cells $N(D)$, containing a mineral deposit D, in the study area consisting of total cells $N(T)$, without taking into account any other information. It can be expressed as

$$P(D) = N(D) \Big/ N(T) \tag{1}$$

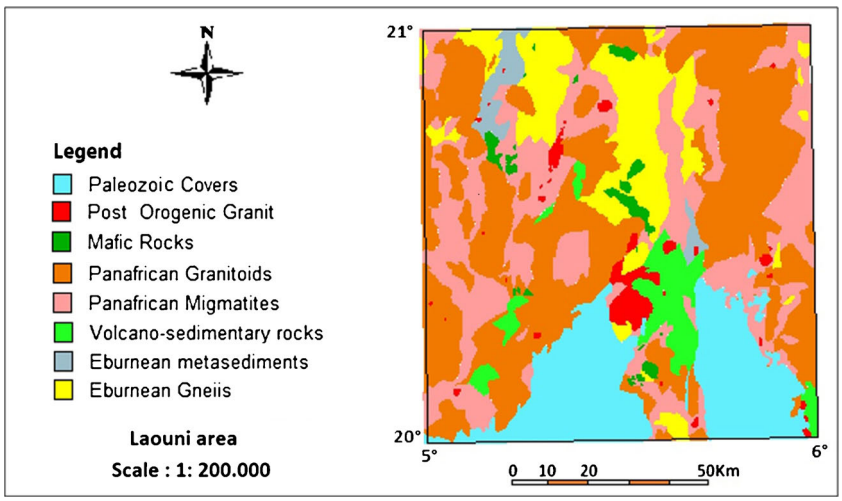

Fig. 2 Simplified geological map of Laouni region

Posterior probability is a revised original probability (prior probability) with the introduction of a new information called evidence. According to Bayesian theorem, it is defined as the probability of occurrence of mineral deposit "*D*" given the presence of the condition *B*1 and noted *P* (*D*|*B*1).

$$P\left(D\middle/B1\right) = P(D)*\frac{P\left(B1\middle/D\right)}{P(B1)} \quad \text{(Bayes theorem)} \tag{2}$$

For "*n*" variables (evidences), Bayesian theorem is expressed in its general form as

$$P\left(D\middle/B\right) = P(D)*\frac{P\left(B1\middle/D\right)}{P(B1)}*\frac{P\left(B2\middle/D\right)}{P(B2)}*\frac{P\left(B3\middle/D\right)}{P(B3)}.....*\frac{P\left(Bn\middle/D\right)}{P(Bn)} \tag{3}$$

The WofE method generally uses a log-linear form of the Bayesian probability to assess the importance of evidence by a pair of weights; the positive weight (W^+) expresses the presence of the evidence *B*, and the negative weight (W^-) its absence denoted $\overline{B}$.

$$W^+ = \mathrm{Ln}\cdot\frac{P\left(B\middle/D\right)}{P\left(B\middle/\overline{D}\right)} = Ln\frac{N(B\cap D)\middle/N(D)}{N\left(B\cap\overline{D}\right)\middle/N\left(\overline{D}\right)} \tag{4}$$

$$W^- = \mathrm{Ln}\cdot\frac{P\left(\overline{B}\middle/D\right)}{P\left(\overline{B}\middle/\overline{D}\right)} = \cdot Ln\frac{N\left(\overline{B}\cap D\right)\middle/N(D)}{N\left(\overline{B}\cap\overline{D}\right)\middle/N\left(\overline{D}\right)} \tag{5}$$

The pairwise of weights (W^+ and W^-) shows *the character of the relationship between the training points and the evidential theme B*. They are calculated for each evidential theme.

The difference between the two weights, known as the contrast, *C*, is also calculated.

$$C = W^+ - W^- \tag{6}$$

The contrast *represents an overall measure of spatial association between the set of deposits D and the evidential theme B*, *combining the effects of the two weights*. For a positive correlation, *C* is positive and *C* is negative in the case of negative spatial correlation.

The studentized contrast or confidence (stud(C)) is also necessary and *expresses a useful measure of the significance of the contrast C and provides an approximate test of the spatial association*, i.e., as an informal test that the contrast *C* is likely to be "real" (Bonham-Carter 1994). It is defined as the ratio of the contrast *C* to its standard deviation (σ).

$$\mathrm{Stud}(C) = C\middle/\sigma \tag{7}$$

The basic idea in the weight of evidence processing is to see which predictor theme shows more deposits in order to suggest that the selected evidential pattern is more predictive and coherent.

Datasets and modeling methodology

Datasets and deposit recognition criterion selection

Datasets used in the current study were mainly extracted from systematic research and geological mapping report (Chillak et al. 1986; unpublished report) enclosing mineral occurrences (deposits, prospects, and mineralized zones), geological map, geochemical anomalies, and tectonic map, whereas airborne radiometric and magnetic data are acquired from "Aéro Service Corporation" (1974) works. All collected raster datasets are georeferenced, digitized, and integrated in GIS environment in order to extract required evidential geoinformation for weights of evidence analysis.

Sn-W-RM mineral occurrences were integrated into the prospectivity analysis as "training sites." Forty-eight mineral occurrences which fall within the study area (Appendix 1) are collected from several bibliographic documents (Armines 1977; Syntchouk et al. 1984; Chillak et al. 1986).

The geochemical anomalies are used to create a "mineralization density map" in order to assess mineral fertility of hosted rock. This map is produced from the distribution of 324 anomalies. The lithological units and tectonic and magmatic layers are derived from various geodatasets and maps. The geophysical data are part of the nationwide airborne magnetic and radiometric coverage of Algeria, flown with line spacing of 2 km. The data were acquired at an elevation of 150 m to provide information about the near-surface geology.

The study area encloses several rare metal deposits such as Nahda, Rechla, Sedis, Tit N'Enir, and Tamazaror. Spatially and genetically, they are associated with the peraluminous related to post-orogenic granitoid, so-called RMGs. The Sn-W-RM mineralization (Appendix 2), enclosing Sn-W, Ta-Nb, Be-Li, La-Ce, Zr, and Bi, are controlled by five ore-controlling factors (deposit recognition criteria): (i) *geology* (lithological units) including gneiss, migmatites, métasédiments, and volcano-clastic rocks; (ii) *tectonic structures*, particularly NE and NW faults, as well as circular structures (Chillak et al. EREM 1986; Al 1990); (iii) *plutonic rocks*, in view of the fact that all Sn-W-RM mineral occurrences are spatially genetically related with "hyper aluminous post-orogenic granites"; (iv) *geochemistry*, because Sn-W-RM geochemical anomalies seem to be an important factor in showing the link between geochemistry fertility and hosted deposit rocks; and (v) *geophysical parameters* given that magnetic and spectrometric signatures (U, Th, and K) can be successfully used to map RMG plutons and identify circular

structures. Thus, the following features representing the basic recognition criteria for our model are

- Location within the appropriate geological unit.
- Location within or around RMG plutons.
- Location near or at the intersection of NE and NW faults and within circular structures.
- Location around or within geochemical Sn-W-RM anomaly zones
- Association with favorable geophysical parameters.

From the existing geodatasets, we have built a GIS database including mineral occurrence layer that represents the training sites and four thematic layers characterizing the geological ore-controlling factors (Fig. 3).

Evidential map generation and spatial analysis

The pixel size used in the present analysis is 1 × 1 km, which is imposed by the scale and the resolution of available geospatial data for the study area. However, the pixel size is considered adequate to represent lateral extension of individual prospects and ensures representation of only one prospect per pixel.

The study area measures 11,570 km^2 or $N\{T\} = 11$, 570 pixels. Multi-class evidential maps were produced for each exploration factor. Most of continuous data were classified into equal-value classes, while to the categorical data, such as the "geological units," a unique attribute value was set to each class.

A proximity analysis (buffering) was performed on faults, circular structures, and RMG plutons where the weighting of a particular feature in the analysis decreases with increasing distance from the feature. Features in each of the evidential maps were buffered at variable intervals. All the evidential maps used in this study that provide information related to the deposit recognition criterion model are given in Figs. 4 and 5.

The spatial association between the derived multi-class evidential layers and the known mineral occurrence were quantitatively analyzed to determine thresholds for binary reclassification. Only classes showing the strongest values of weights and characterized by good confidence were retained as predictor pattern.

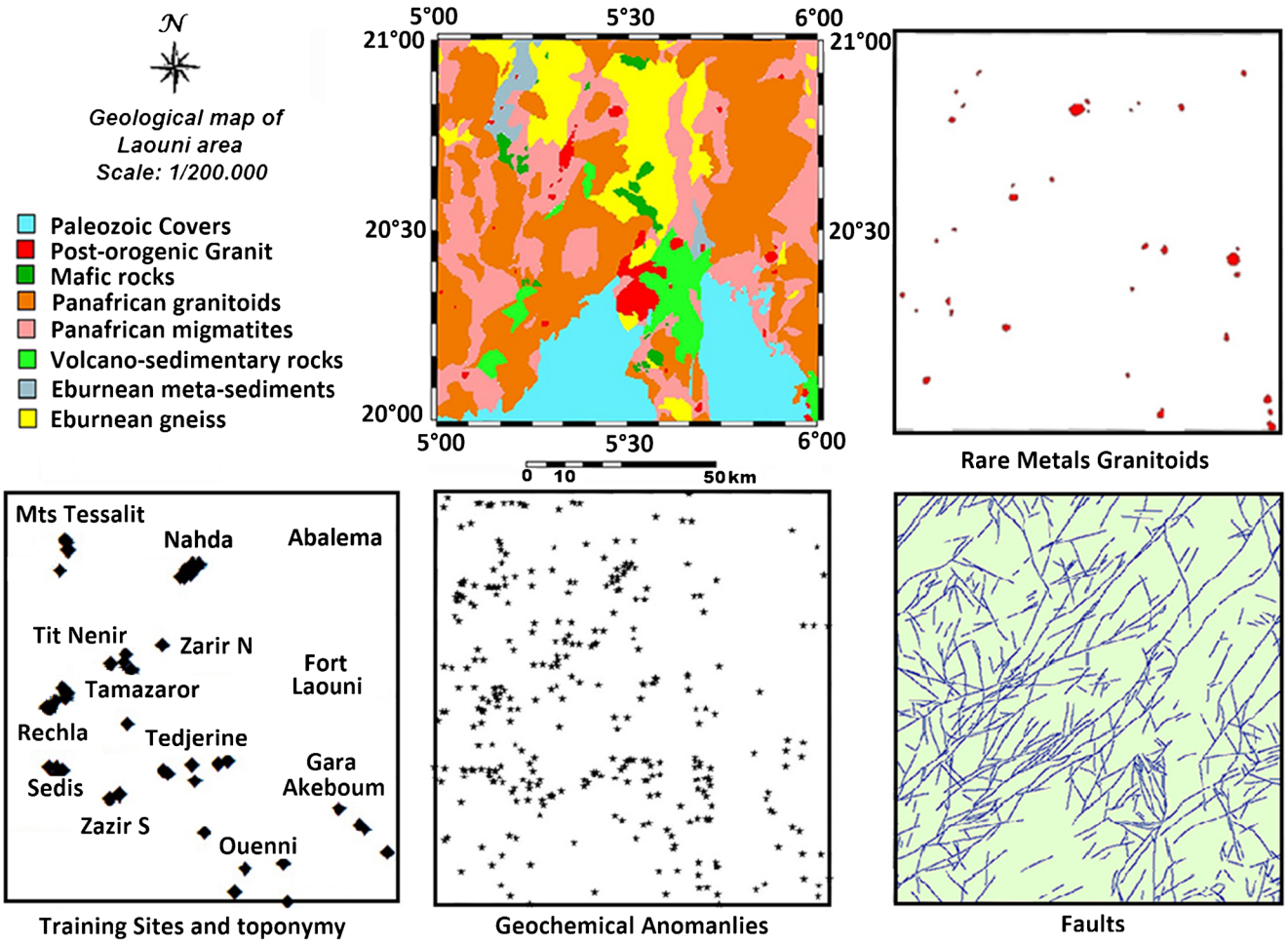

Fig. 3 Geological evidential themes digitized from raster datasets

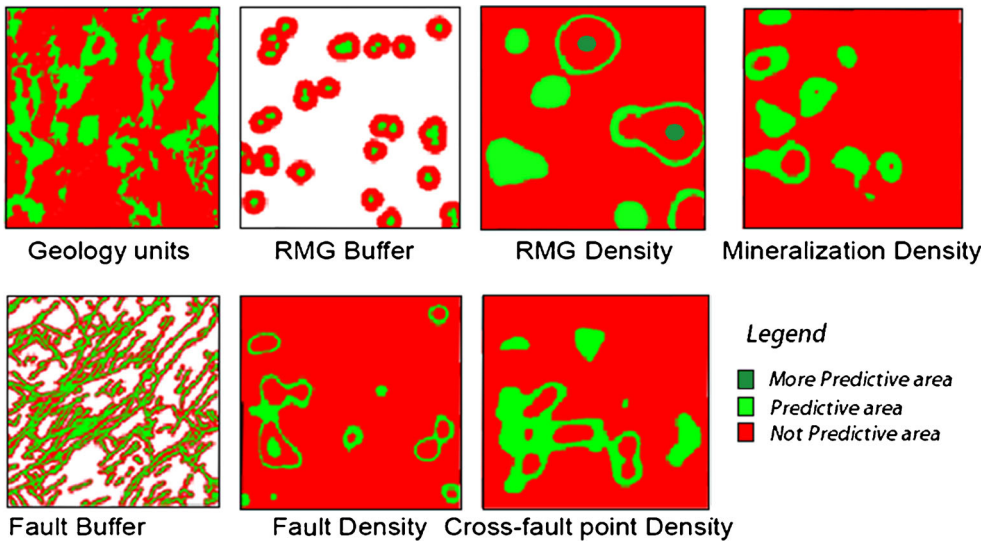

Fig. 4 Binary predictor maps derived from geological data

The following table shows an example of the calculated weights related to the spatial association between the "lithological units" and training sites (Table 1).

As expected, the strongest positive values of W^+, contrast and confidence, correspond to RMG class (class 2). Thus, RMG can be taken as the best predictive geological unit, in addition to the "*migmatite PR1*" unit (class 4) which seems also to be a suitable lithological predictor unit as expressed by a positive contrast (0.6335) and a good value of confidence (2.1193). In the reclassified lithological evidential binary theme, these two units were assembled together to form a single predictive class, and the weights of evidence parameters were recalculated (Table 2).

In the same way, all of the *themes* were treated, and after analyzing their weights of evidence statistical parameters, the other binary predictor themes have been weighted, analyzed, and reclassified into binary maps.

Weights of evidence modeling results

The WofE modeling requires the combination of all generated binary predictor maps. Modeling without checking with statistical test of conditional independence (CI), a preliminary generated MPM causes an overestimation or underestimation

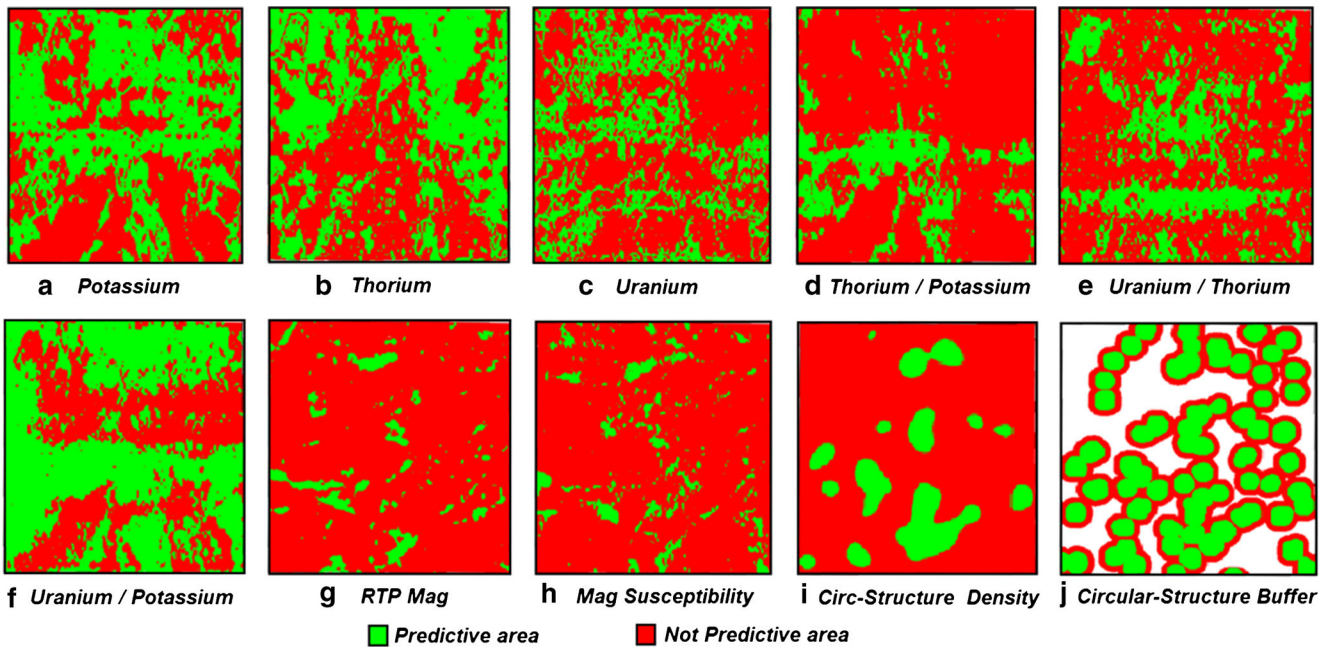

Fig. 5 Binary predictor maps derived from airborne geophysical data

Table 1 Summary of "lithological units" of WofE calculation parameters

Class	Unité_geol	Area	Points	W+	s (W+)	W−	s (W−)	Contrast	s (C)	Stud(C)
1	Gneiss PR1	1376	0							
2	Granite PO	244	9	2.2192	0.3397	−0.1870	0.1604	2.4063	0.3756	6.4060
3	Gr_migm	4415	14	−0.2689	0.2677	0.1359	0.1719	−0.4048	0.3181	−1.2725
4	MigmPR1	2803	18	0.4400	0.2365	−0.1936	0.1829	0.6335	0.2989	2.1193
5	MétasedPR1	221	0							
6	Paleozoic	1838	5	−0.4227	0.4478	0.0631	0.1528	−0.4858	0.4732	−1.0267
7	R_basique	162	0							
8	Volc-Terr	515	2	−0.0655	0.7085	0.0029	0.1477	−0.0685	0.7237	−0.0946

of posterior probability induced by conditional dependence between maps.

In practice, the combined maps are not completely independent and always present some degree of dependence to one another (Bonham-Carter 1994; Mihalasky 1999; Porwal and Halle 2003). Thus, CI is always violated to some degree. Therefore, the geomodeler must assess the severity of the violation and try to identify the maps that are causing CI problems so they can be rejected from the final analysis. To overcome such a problem, various tests for CI were suggested; the first one is pairwise test for CI that calculates χ^2 (chi-squared) statistic value where for 1 *df* and 95 % of probability level $\chi^2 = 3.8$ rejects the CI test (Bonham-Carter 1994). The second one is the original overall test (OT). If $95 > OT > 0.85$, CI is not violated seriously. The last one is the new omnibus test (NOT) that is more effective, not subject to limitation, and is applied even in areas with large or small number of training points (Bonham-Carter et al. 1989; Paganelli et al. 2002; Agterberg et al. 1993; Wright and Bonham-Carter 1996; Carranza and Hale 2000, 2002; Thiart et al. 2007). In this case, the CI hypothesis is accepted if $85 < NOT < 95$ %.

CI test results, obtained for the preliminary model, cannot be represented here because of its voluminous contingency table which indicates a number of CI problems between some layers. To overcome this difficulty, we separate the predictor maps into two intermediate models, geological and geophysical predictor maps.

Geological predictor patterns and CI tests

The geological model consists of seven binary predictor maps which have been checked with the CI test. The contingency table results, given in Table 3, illustrate clearly some degree of dependence between predictor maps 1 and 2 ("intersection fault point density pattern" and "fault density pattern") and other maps as shown by the calculated high values of χ^2 and low values of its corresponding probability. Then, the final modeling requires the rejection of these two maps.

Geophysical predictor patterns and CI tests

The geophysical predictor patterns consist of ten predictor patterns including uranium (U), thorium (Th), potassium (K), U/Th, U/K, and Th/K, all well expressed by their respective binary predictor maps (Fig. 5). These patterns were also assessed using the CI test. The CI contingency table results (Table 4) show clearly that "circular structure density" (map 9) causes a serious CI problem as well as the U/K theme (map 6) as shown by the high values of χ^2 and their low corresponding probability values. Their rejection from the final model seems to be necessary.

WofE modeling and cross validation

Modeling without CI problematic layers, we obtain a more coherent model enclosing only 11 evidences. The CI test contingency table indicates acceptable values of probabilities and chi-squared (Table 5). The MPM, obtained from this model and represented in Fig. 6, was reclassified into the following three classes: prospective, less prospective, and not prospective areas.

Control of the modeling results using "deposit tests"

In order to test the predictive accuracy of our exploration modeling pattern, a control model was generated using only 40 of the 48 training sites previously used. Eight mineral occurrences (no. 28, 29, 30, 31, 32, and 34; bold in Table 6), representing the best

Table 2 Weights of the binary reclassified lithological theme

Class_By_Wt	Description	Area	Points	W+	s (W+)	W−	s (W−)	Contrast	s (C)	Stud(C)
Inside 1	Predictive	3048	27	0.7641	0.1933	−0.5229	0.2185	1.2870	0.2917	4.4116
Outside 2	Not predictive	8531	21	−0.5229	0.2185	0.7641	0.1933	−1.2870	0.2917	−4.4116

Table 3 Contingency table for CI test for the geological model

		1	2	3	4	5	6
Probability							
Buf_Fa_CrossNE_NW_Class	7	0,92116	0,69526	0,27422	0,65804	0,84308	0,5255
Fa_IntersPt_Dens_Class	1		0,00598	0,55861	0,8827	0	0,00285
Fault_Density_Class	2			0,01915	0,0228	0,00598	0,57841
GMR_RBuf_Clas	3				0,03882	0,80402	0,68014
Geo_Class	4					0,8827	0,74321
MinDensity_Class	5						0,06606
RMG_Density_Class	6						
Probabilities >0.05 indicate pairwise CI							
Probability values depend on chi-squared and degrees of freedom							
Chi-squared							
Buf_Fa_CrossNE_NW_Class	7	0,01	0,153	1,196	0,196	0,039	0,403
Fa_IntersPt_Dens_Class	1		7,519	0,342	0,022	23,52	8,875
Fault_Density_Class	2			5,429	5,121	7,519	0,309
GMR_RBuf_Clas	3				4,186	0,062	0,17
Geo_Class	4					0,022	0,107
MinDensity_Class	5						3,265
RMG_Density_Class	6						
Degrees of freedom = 1 for all pairwise predictor maps							
New overall test of CI = 0.00	Probability of 0.5000						

The underlined numbers indicate conditional dependance between combined layers

deposits of Nahda region, were retired from training sites in this analysis. The posterior probability map, obtained from this model (Fig. 7), shows comparable results as the previous MPM, and efficiently predicts the locations of the well-known deposits of

Table 4 Contingency table for CI test for the geophysical model

		1	2	3	4	5	6	7	8	9
Probability										
K_Class1	10	0,19771	0,40095	0,70766	0,05895	0,5048	0,0295	0,32876	0,93622	0,19543
Mag_Der_Class1	1		0,23778	0,35474	0,91927	0,8686	0,77245	0,06773	0,626	0,13652
Mag_Susc_Clas	2			0,654	0,02802	0,85732	0,72367	0,73065	0,46334	0,85732
Str_CircBuf_CalsCum3					0,17874	0,74223	0,00555	0,88123	0,35391	0
ThK_Class1	4					0,12648	0,02035	0,79023	0,59253	0,15114
Th_Class3	5						0,74118	0,4693	0,44086	0,58516
UK_Class1	6							0,0544	0,21683	0,00291
UTh_Lao_Class	7								0,86974	0,57356
U_Class		8								0,14544
Str_Circ_Density	9									
Chi-squared										
K_Class1	10	1,659	0,705	0,141	3,461	0,445	4,667	0,954	0,006	1,676
Mag_Der_Class1	1		1,394	0,856	0,01	0,027	0,084	3,222	0,238	2,217
Mag_Susc_Clas	2			0,201	4,757	0,032	0,125	0,119	0,538	0,032
Str_CircBuf_CalsCum	3				1,808	0,108	7,656	0,022	0,859	26,428
ThK_Class1	4					2,335	5,322	0,071	0,286	2,061
Th_Class3	5						0,109	0,524	0,594	0,298
UK_Class1	6							3,6	1,525	8,836
UTh_Lao_Class	7								0,027	0,317
U_Class	8									2,119
Str_Circ_Density	9									

The underlined numbers indicate conditional dependance between layers

Degrees of freedom = 1 for all pairwise layers, original overall test of CI = 0.77 CI may not hold if value < 0.85, and new overall test of CI = 0.00 probability of 0.4984

Table 5 Contingency table for CI test without problematic predictor maps

		1	2	3	4	5	6	7	8	9	10
Probability											
K_Class1	11	0,19771	0,40095	0,1046	0,13176	0,74321	0,7077	0,05895	0,5048	0,32876	0,93622
Mag_Der_Class1	1		0,23778	0,72962	0,1289	0,07333	0,3547	0,91927	0,8686	0,06773	0,6261
Mag_Susc_Clas	2			0,31049	0,85675	0,86752	0,654	0,02802	0,85732	0,73065	0,46334
MinDensity_Class	3				0,79573	0,06606	0,7076	0,45047	0,269	0,13057	0,28303
RBuf_Fa_NE_NW_Class	4					0,13999	0,8134	0,10238	0,90012	0,60324	0,60588
RMG_Density_Class	5						0,8226	0,87482	0,84555	0,2047	0,44244
Str_CircBuf_CalsCum	6							0,17874	0,74223	0,88123	0,35391
ThK_Class1	7								0,12648	0,7902	0,59253
Th_Class3	8									0,4693	0,44086
UTh_Lao_Class	9										0,86974
U_Class	01										
Chi-squared											
K_Class1	11	1,659	0,705	2,634	2,272	0,107	0,141	3,461	0,445	0,954	0,006
Mag_Der_Class1	1		1,394	0,119	2,306	3,086	0,856	0,015	0,027	3,222	0,238
Mag_Susc_Clas	2			1,029	0,033	0,028	0,201	4,757	0,032	0,119	0,538
MinDensity_Class	3				0,067	3,265	0,141	0,569	1,222	2,286	1,152
RBuf_Fa_NE_NW_Class	4					2,178	0,056	2,668	0,016	0,271	0,266
RMG_Density_Class	5						0,052	0,025	0,038	1,608	0,590
Str_CircBuf_CalsCum	6							1,808	0,108	0,022	0,859
ThK_Class1		7							2,335	0,071	0,286
Th_Class3		8								0,524	0,594
UTh_Lao_Class		9									0,027
U_Class			10								

Degrees of freedom = 1 for all pairwise layers, original overall test of CI = 0.86 CI may not hold if value < 0.85, and new overall test of CI = 0.01 probability of 0.5

Nahda, validating the consistency and effectiveness of the used exploration model. This reveals a large success of the weights of evidence modeling applied for Sn-W-RM prediction in this region.

Conclusions and perspectives

The GIS-based "weights of evidence" approach, carried out step by step using MapInfo-SDM, was successfully applied in the Laouni area. The existing deposits are used as training sites and geodatasets as predictor patterns describing the deposit recognition criterion model of Sn-W-RM of RMG deposit-type sought.

According to the WofE modeling: (1) we have *built a digital database* including a training site layer including 48 mineral occurrences and five thematic layers representing the RMG deposit recognition criterion model (lithology, faulting, magmatism, geochemistry, and geophysics), all collected from diverse geodata, digitized, and integrated into a GIS environment. (2) Seventeen binary predictor maps were derived from the thematic layers, weighted to select the best of them, and are combined to *generate a preliminary posterior probability map*. (3) The obtained model was checked for the CI test, and six problematic layers were deleted from the final modeling. (4) The retained coherent evidential layers were combined in the final model to generate a valid posterior probability map representing the "mineral prospectivity map" for Laouni, showing the following three main areas: predictive, less predictive, and not predictive areas. (5) The permissive areas, *reduced to a small surface*, include more than 30/48 mineral occurrences and represent the *most predictive zones* for Sn-W-RM in our region. (6) The MPM generated shows *several underexplored areas* (Zazir S, Zazir N, Fort Laouni, North Rechla, South Ouenni, Akeboum, and Tedjerine region) and *unrecognized favorable areas* such as the Mounts of Tessalit.

In order to assess the accuracy of the WofE modeling, we have produced a *controlling model* where eight of the top deposits of Nahda region were excluded from this model. The MPM reveals similar results: (1) the location of the permissive area is globally comparable with the previous model, (2) the permissive area includes several known deposits (more than 20 deposits) and strongly predicts the known mineralized zone of Nahda region, and (3) the control WofE model can be extended to the adjacent regions of the study area which enclose a small number of deposits.

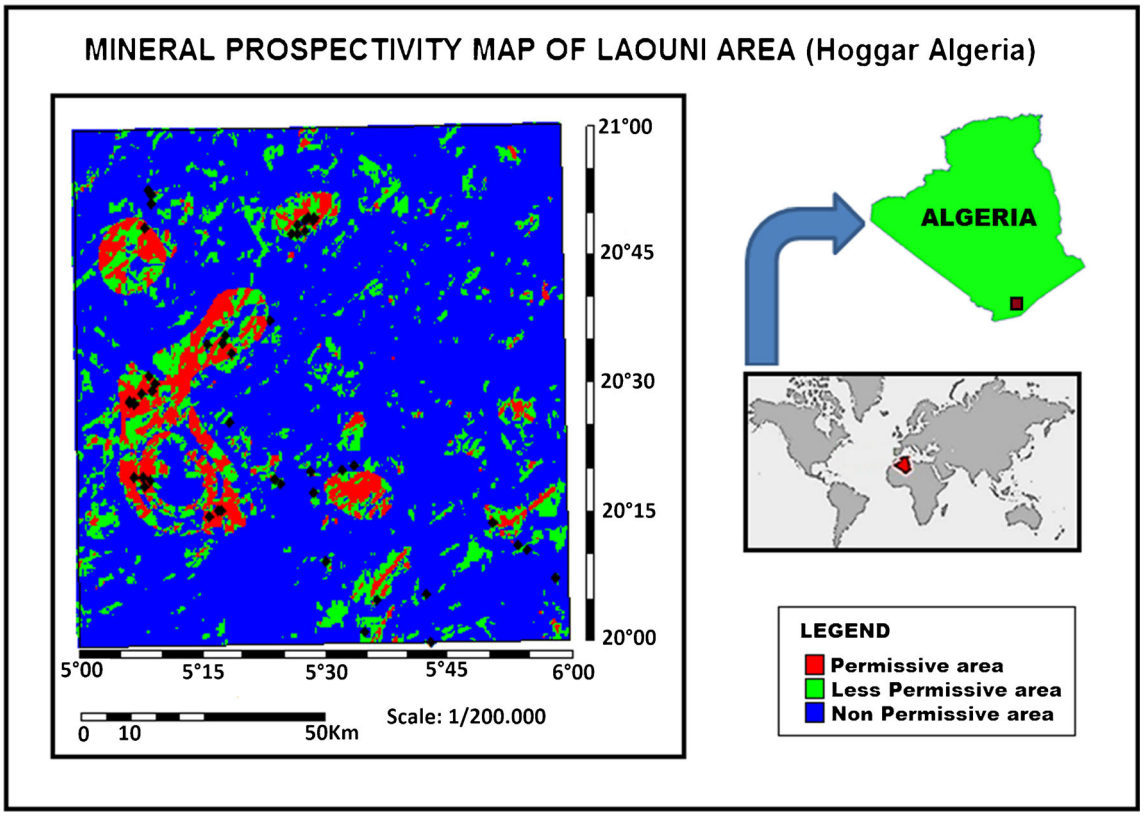

Fig. 6 Mineral prospectivity map for Sn-W-RM of Laouni study area

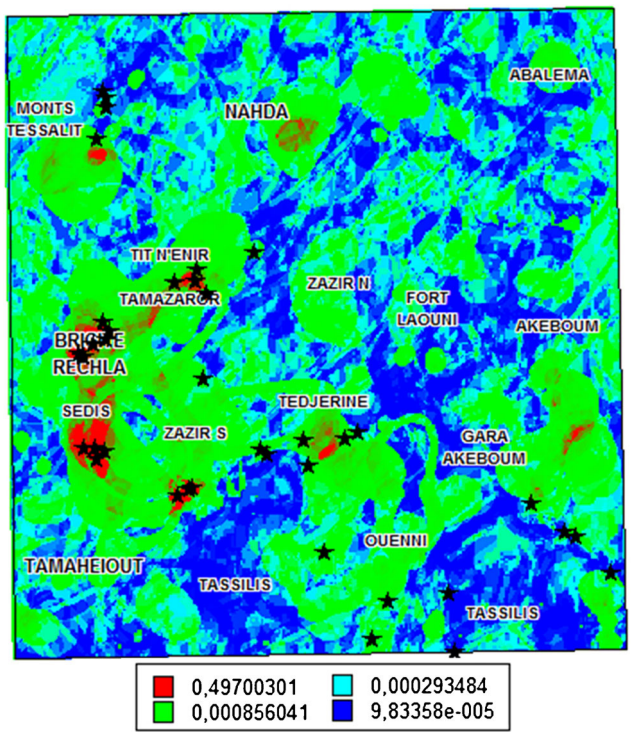

Fig. 7 MPM control indicating the prediction of the well-known deposits of Nahda

In the light of these evident results, the GIS-based WofE modeling, combining known mineral deposits and geodatasets, provides an improved tool for mineral potential mapping of Sn-W and rare metals of the Laouni region. This modeling allowed the demonstration of the capability of the multi-source spatial analysis and the accuracy of the data-driven methods applied to a region where deposit recognition criteria are well known. The suitability of the results is equally supported by the location of the well-known deposits of Nahda, Sedis, Rechla, and Tit N'Enir and by the prediction of underexplored areas such as Ouenni, Akeboum, and Tessalit Mount regions.

On the other hand, the WofE modeling led to confirm the use of some adequate ore-controlling factors by the quantitative analysis of their spatial association with the known deposits. A number of them (e.g., association with RMG plutons and NE-NW faults) are well known and previously used by mineral explorers as main ore-controlling factors, whereas other new possible features are recognized (association with migmatitic rocks and association with specific values of magnetic susceptibility). Therefore, the WofE approach is highly recommended in the future for mineral exploration projects of Sn-W and rare metal mineralization in the Hoggar area, especially where airborne geophysical data exists.

Appendix 1

Table 6 Training site table

Deposit	Name	*X*	*Y*	Prim Elt	Sec Elts	Host rock	Genetic type
1 Dep	Rechla	5.1125	20.375	Ta, Nb, Sn	–	PO granite	Magmatic
2 Show	–	5.1525	20.4778	Ta, Li	Sn, Be	Pegmatite-greisen	Hydrothermal
3 Show	–	5.11944	20.3292	W	Sn	Filon de Qz	Hydrothermal
4 Dep	–	5.12	20.4722	W, Sn	Be, Li	Greisen	Hydrothermal
5 Adv prosp	Rechla	5.12083	20.4708	W, Sn	Be, Li	PO granite	Magmatic
6 Dep	Antar	5.13611	20.4917	Be, Sn, W	–	Granite métasom	Magmatic
7 Show	–	5.13889	20.3278	Be	Nb, Ta, Sn, Li	Granite gréisen	Pneumatic-hydrothermal
8 Dep	Sedis N	5.13944	20.3106	Ta	–	PO granite	Magmatic
9 Dep	Tessalit	5.14583	20.8111	Be	–	PO granite	Magmatic
10 Adv prosp Sedis		5.15278	20.3236	W, Sn	Be, Li	Greisen	Magmatic
11 Show	Brigitte	5.15278	20.625	Be	–	PO granite	Magmatic
12 Dep	–	5.158	20.497	Sn	Li, Be, W	Greisen	Hydrothermal
13 Show	Brigitte	5.15833	20.8833	Ag, W	Sn	Filon de Qz	Hydrothermal
14 Show	Colline noire	5.1625	20.375	W	–	Pegmatite-Qzvein	Hydrothermal
15 Dep	Tessalit	5.16389	20.5583	Be	Sn, Li, Bi	Skarn + pegmatite	Hydrothermal
16 Show	–	5.16389	20.9111	Sn	Li, Ag	Greisen	Hydrothermal
17 Dep	Tit N'EnirE	5.27222	20.5847	Sn, W	–	PO granite	Magmatic
18 Show	–	5.27222	20.2528	Zr	–	Schiste silicifié	Hydrothermal
19 Show	–	5.29167	20.2225	Be	Sn, Li, Nb, Y, Yb	Granite greisenisé	Pneumatic-hydrothermal
20 Show	–	5.29583	20.2639	Nb	Y, Yb, Zr	Filon de pegmatite	Pégmatitique
21 Dep	Tit N'EnirN	5.30556	20.5875	Be	–	PO granite	Magmatic
22 Show	–	5.30972	20.8028	Sn	–	Granite-pégmatite	Magmatic
23 Adv prosp	Tamazaror	5.31667	20.4333	Ta, Nb	Sn, Li, Be, Ge	PO granite	Magmatic
24 Adv prosp	Tit N'Enir	5.32361	20.5667	Sn, W	Li, Bi	Filon de Qz	Hydrothermal
25 Show	–	5.40417	20.6292	Sn	Li	Grésen	Hydrothermal
26 Show	–	5.40833	20.3222	Zr	Mo, V	Zone silicifiée	Hydrothermal
27 Show	–	5.41944	20.3139	Zr	Y, Yb, La, Tr	Zone silicifiée	Hydrothermal
28 Show	–	**5.45**	**20.7958**	**W**	–	**Stockwerk**	**Hydrothermal**
29 Dep	**Monticule**	**5.46111**	**20.8125**	**W**	–	**Greisen + Qzvein**	**Hydrothermal**
30 Show	–	**5.4625**	**20.7958**	**Be**	**Sn, Li**	**Filon de pegmatite**	**Hydrothermal**
31 Dep	–	**5.47639**	**20.8222**	**W**	–	**Filons de Qz**	**Hydrothermal**
32 Dep	**Nahda S**	**5.47639**	**20.8033**	**Be**	**Ta, Nb, Sn**	**Filon de pegmatite**	**Pégmatitique**
33 Dep	–	5.48056	20.3361	Nb	Y, Yb, Zr	Granite gréisenisé	Magmatic
34 Dep	–	**5.48333**	**20.8292**	**W**	–	**Stockwerk**	**Hydrothermal**
35 Show	–	5.4875	20.2958	Zr	Y, Nb, Sn	Zone silicifiée	Hydrothermal
36 Dep	**Filon doux**	**5.49306**	**20.8222**	**W**	–	**Filon de pegmatite**	**Magmatic**
37 Adv prosp	**Nahda**	**5.49583**	**20.8292**	**Sn, W**	**Mo, Cu, Au, Li**	**Qzvein-greisen**	**Hydrothermal**
38 Show	–	5.51111	20.1611	La, Zr	Ce, Nb, Be, Au	Zone silicifiée	Téléthermal
39 Show	–	5.54611	20.3375	Sn	Li	Granite gréisenisé	Hydrothermal
40 Show	–	5.56944	20.3458	Sn	Y, Yb, Nb, Zr	Granite gréisenisé	Magmatic
41 Show	–	5.5875	20.025	La, Ce	Th, U, Y, Yb, Zr	Zone silicifié	Téléthermal
42 Show	–	5.61389	20.0833	Nb	Y, Yb	Filon de pegmatite	Pégmatitique
43 Show	–	5.71389	20.0944	Zr, La	Y, Nb, Sn	Zone silicifiée	Téléthermal
44 Show	–	5.72222	20.0028	La, Ce	Y, Yb, Zr	Zone silicifiée	Téléthermal
45 Dep	–	5.85139	20.2306	W	–	Granite greisenisé	Hydrothermal
46 Show	–	5.90417	20.1875	La, Zr	Sm, Y, Yb, Th	Zone silicifiée	Hydrothermal
47 Show	–	5.92167	20.1778	Nb, Zr	Y, Ce, Sn	Zone silicifiée	Hydrothermal
48 Show	–	5.97778	20.1222	Bi	Ag, Cu	Zone silicifiée	Hydrothermal

The bold lines represent a control set of deposits that were not used in processing but that are used to validate the results

Show showing, *Dep* deposit, *Ad prosp* advanced prospect

Appendix 2: Main abbreviations used in text

MPM	Mineral potential map (mineral prospectivity map)
GIS	Geographical Information System
Sn-W-RM	Tin, wolfram, and rare metals
SDMS	Spatial data modeler
WofE	Weights of evidence
ANN	Artificial neural network
AP	Anterior probability
PP	Posterior probability
RMG	Rare metal granitoid
PO	Post-orogenic
CI	Conditional independence

References

Agterberg FP, Bonham-Carter GF, Cheng Q, Wright DF (1993) Weights of evidence modeling and weighted logistic regression in mineral potential mapping. In: Davis JC, Herzfeld UC (eds) Computers in geology. Oxford University Press, New York, pp 13–32

Bellov and Al (1990) Rapport sur les résultats des travaux thématiques effectués par le groupe "Taourirt" en 1987–1989 au Hoggar. E.re.m 1990; Unpublished report

Armines (1977) Inventaire et prospective des ressources minérales du Hoggar, Alger 1977

Azzouni-Sekkal A (1990) Petrologie et geochimie des granites de type "Taourirt": un exemple de province magmatique de transition entre les regimes orogeniques et anorogeniques, au Panafricain (Hoggar-Algerie). These USTHB, Alger, 667 pp. and Memoire Service Geologique Algerie, 1995, 7, Boumerdes, 288 pp

Barbieri G, Cambuli P (2009) The weight of evidence statistical method in landslide susceptibility mapping of the Rio Pardu Valley (Sardinia, Italy) 18th World IMACS / MODSIM Congress, Cairns, Australia 13–17

Benazouz-Fezoui A (1989) Pétrologie des granites Taourirts et pegmatites associées de la région de Laouni (Hoggar Central méridional). Contribution à l'explication de certains processus tardi et post-magmatiques originaux. Thèse de Magister, IST/USTHB, Alger. 195p

Benomar TB, Fuling B (2006) Predictive GIS model for potential mapping of Cu, Pb, Zn mineralization. Geospatial Inf Sci Q 9(2)

Bertrand JML, Caby R (1978) Geodynamic evolution of the Pan-African orogenic belt: a new interpretation of the Hoggar shield (Algerian Sahara). GeologischeRundschau 67:357–388

Bertrand JML, Michard A, Boullier AM, Dautel D (1986) Structure and U/Pb geochronology of Central Hoggar (Algeria): a reappraisal of its Pan-African evolution. Tectonics 5:955–972

Black R, Caby R, Moussine-Pouchkine A, Bayer R, Bertrand JML, Boullier AM, Fabre J, Lesquer A (1979) Evidence for late Precambrian plate tectonics in West Africa. Nature 278:223–227

Black R, Latouche L, Liegeois JP, Caby R, Bertrand JM (1994) Pan-African displaced terranes in the Tuareg shield (central Sahara). Geology 22:641–644

Boissonnas J (1973) Les granites à structure concentriques et quelques autres granites Tardifs de la chaîne panafricaine en Ahaggar (Sahara central, Algérie).Thèse Doctorat es-Sciences, Centre de Recherches sur les Zones Arides, Série Géologie 16, 662 p

Bonham-Carter GF (1994) Geographic information systems for geoscientists. Modeling with GIS. Computer methods in the geosciences 13. Pergamon, Oxford, p 398

Bonham-Carter GF, Agterberg FP, Wright DF (1989) Weights of evidence modeling: a new approach to mapping mineral potential, in F. P. Agterberg and Bonham-Carter (Eds.), Statistical Applications in the Earth Sciences: Geological Survey Canada Paper 89–9, p. 171–183

Caby R, Bertrand JML, Black R (1981) Oceanic closure and continental collision in the Hoggar-Iforas Pan-African segment. In: A. Kröner, (Ed.), Precambrian Plate Tectonics. Elsevier, pp. 407–434

Carranza EJM (2009) Geochemical anomaly and mineral prospectivity mapping in GIS, Handbook if exploration and environmental geochemistry 11. Elsevier, UK, p 351

Carranza EJM, Hale M (2000) Spatial association of mineral occurrences and curvi-linear geological features. Math Geol 34: 199–217

Carranza EJM, Hale M (2002) Geologically constrained probabilistic mapping of gold potential, Baguio District, Philippines. Nat Resour Res 9:237–253

Chalal Y (1989) Contribution à l'étude de la greïsénisation et des minéralisations wolframifères associées aux granites de Tamazaror et de Sedis, Laouni, Hoggar Central. Caractérisation pétrologique, géochimique et implications métallogéniques. Thèse de Magister, IST / USTHB, Alger. 252 p

Chillak et al. EREM (1986) Rapport final sur les recherches systématiques et le levé géologique au 1/200 000 effectués au sud du Hoggar central sur les feuilles Laouni In Atei et In Guezzam. ORGM, rapport inédit. ORGM, rapport inédit

Cottin JY, Lorand JP, Agrinier P, Bodinier JL, Liègeois JP (1998) Isotopic (O, Sr, Nd) and trace element geochemistry of the Laouni layered intrusions (Pan-African belt, Hoggar, Algeria): evidence for post-collisional tholeitic magmas variably contaminated by continental crust. Lithos 45:197–222

Diggs D, Brunswig R (2010) Weights of evidence modeling in archeology, Rocky Mountain, National park, School of social science Colleges of humanities and social sciences University of Northern Colorado Greeley, Colorado

Djadoun A (1993) Contribution à l'étude des granites alumineux (Hoggar Central) à l'exemple des massifs d'Alous Ouan Rechla, Tit-En-Enir, Tamazaror. Aspect minéralogique, géochimique et considérations pétro-génétiques. Thèse de Magister IST/USTHB, Alger, 233p

Fagin TD, Hoagland Bruce W (2010) Patterns from the past: modeling Public Land Survey witness tree distributions with weights-of-evidence. Plant Ecol. doi:10.1007/s11258-010-9815-9

Harris J, Wilkinson L, Heather K, Fumerton S, Bernier M, Ayer J, Dahn R (2001) Application of GIS processing techniques for producing mineral prospectivity maps—a case study: mesothermal Au in the Swayze Greenstone Belt, Ontario, Canada. Nat Resour Res 10(2): 91–124

Hyun-Joo O, Saro L (2010) Landslide susceptibility mapping on Panaon Island, Philippines using a geographic information system. Environ Earth Sci. doi:10.1007/s12665-010-0579-2

Kesraoui M (2006) Nature et évolutions comparées de granites à métaux rares dans le Hoggar Central (Algérie) à travers la pétrographie, la cristallochimie des micas et des minéraux à Ta, Nb, Sn, W. et la géochimie. Thèse Doctorat d'Etat, FSTGAT /USTHB, Alger. 237 p

Lelubre M (1952) Recherches sur la géologie de l'Ahaggar central et occidental (Sahara Central). Bulletin Service Carte Géologique Algérie, 2ème série, 22, 2 tomes

Liegeois JP, Latouche L, Boughrara M, Navez J, Guiraud M (2003) The LATEA metacraton (central Hoggar, Tuareg shield, Algeria): behavior of an old passive margin during the Pan-African orogeny. J Earth Sci. 37

Mathew J, Jha K, Rawat GS (2007) Weights of evidence modeling for landslide hazard zonation mapping in part of Bhagirathi valley, Uttarakhand. Curr Sci 92(5)

Mihalasky (1999) Mineral potential mapping of gold and silver mineralization in Nevada Great basin, a GIS Based analysis using WofE method. PhD thesis Abstract: Department of earth sciences university of Ottawa Last acceded Sept 24 2001

Nykänen V, Salmirinne H (2007) Prospectivity analysis of gold using regional geophysical and geochemical data from the central Lapland greenstone belt, Finland; Gold in the Central Lapland Greenstone Belt, Finland V. Juhani Ojala (ed.) Geological survey of Finland, Special Paper 44, 251– 269, 2007

Nykänen V, Karinen T, Niiranen T, Lahti J (2011) Modeling the gold potential of central Lapland, northern Finland Geoscience for Society 125th Anniversary Volume Edited by Keijo Nenonen and Pekka A. Nurmi Geological Survey of Finland, Special Paper 49, 71–82, 2011

Paganelli F, Richards JP, Grunsky EC (2002) Integration of structural, gravity, and magnetic data using the weights of evidence method as a tool for kimberlites exploration in the Buffalo Head Hills, Northern Central Alberta, Canada. Nat Resour Res 11(3):219–236

Partington G (2010) Developing models using GIS to assess geological and economic risk: An example from VMS copper gold mineral exploration in Oman Kenex Pty Ltd, PO Box 2145, Marmion, WA 6020, Australia. Ore Geol Rev 38(2010):197–207

Porwal C, Halle (2003) Extended weights-of-evidence modelling for predictive mapping of base-metal deposit potential in Aravalli Province, western India. Explor Min Geol 10(4):155–163

Porwal A, Carranza EJM, Hale M (2001) Extended weights-of-evidence modelling for predictive mapping of base metal deposit potential in Aravalli Province, western India. Explor Mining Geol 10(4):273–287

Porwal A, Carranza EJM, Hale M (2006a) Bayesian network classifiers for mineral potential mapping. Comput Geosci 32(1):1–16

Porwal A, Carranza EJM, Hale M (2006) A hybrid fuzzy weights-of-evidence model for mineral potential mapping; Natural Resources Research (2006). doi:10.1007/s11053-006-9012-7

Romero-Calcerrada R, Novillo CJ, Millington JDA, Gomez-Jimenez I (2008) GIS analysis of spatial patterns of human-caused wildfire ignition risk in the SW of Madrid (Central Spain). Landsc Ecol 23: 341–354. doi:10.1007/s10980-008-9190-2

Syntchouk et al (1984) Notice explicative de la carte des formations géologique et de la carte d'inventaire des gites minéraux, carte de l'interprétation des champs géophysiques et carte métallogénique prévisionnelle, carte prévisionnelle et de recommandations au 1: 500 000. Alger, 1984

Thiart C, Bonham-Carter GF, Agterberg FP (2007) Conditional independence in weights-of-evidence: application of an improved test. Proceedings, 9th Conference of the International Association for Mathematical Geology, held in Portsmouth, U.K., September 2003 (Proceedings on CD-ROM)

Wang H, Al (2002) Data integration using weights of evidence method, application in mapping mineral potential resources ISPRS, Commission group IV, Working group IV/7

Wildman C, and Peters K, (2008) A predictive model for identifying the potential location of Powelliphanta land snails in the south island of new Zealand, Kenex Knowledge Systems

Wright DF, Bonham-Carter GF (1996) VHMS favorability mapping with GIS-based integration models, Chisel Lake–Anderson Lake area. In: Bonham-Carter GF, Galley AG, Hall GEM (eds) EXTECH I: a multidisciplinary approach to massive sulphide research in the Rusty Lake–Snow Lake Greenstone Belts, Manitoba. Geological Survey of Canada Bulletin 426, pp 339–376, 387–401

Yousefi M, Kamkar-Rouhani A (2004) Modelling of mineral potentials of gold and base metals using GIS in Mahneshan area, Iran) 2

Zhang D, Cheng Q, Agterberg FP, Zuo R (2014) A comparison of modified fuzzy weights of evidence, fuzzy weights of evidence, and logistic regression for mapping mineral prospectivity. Math Geosci 46:869–885

Ziaii M, Pouyan A, Ziaei M (2009) A computational optimized extended model for mineral potential mapping based on WofE method. Am J Appl Sci 6(2):200–203, ISSN 1546–9239 © 2009 Science Publications

Zuo R, Zhang Z, Zhang D, Carranza EJM, Wang H (2015) Evaluation of uncertainty in mineral prospectivity mapping due to missing evidence: a case study with skarn-type Fe deposits in southwestern Fujian Province, China. Ore Geol Rev 71:502–515